Supporting Information:

Morphology Dynamics of Single-layered $Ni(OH)_2$/NiOOH Nanosheets and Subsequent Fe Incorporation Studied by *in-situ* Electrochemical Atomic Force Microscopy

Jiang Deng,[1] Michael R. Nellist,[2] Michaela Burke Stevens,[2,#] Christian Dette,[2] Yong Wang,[1] and Shannon W. Boettcher[2,*]

[1]Advanced Materials and Catalysis Group, Center for Chemistry of High-performance and Novel Materials, Department of Chemistry, Zhejiang University, Hangzhou, 310028, P. R. China.

[2]Department of Chemistry and Biochemistry, University of Oregon, Eugene, Oregon 97403, United States

*E-mail: swb@uoregon.edu

[#]Present address: Department of Chemical Engineering, Stanford University, Stanford, CA 94305, United States

Experimental section:

Materials and reagents. $Ni(NO_3)_2 \cdot 6H_2O$ (98%, Alfa Aesar), sodium dodecyl sulfate (SDS, Fisher Scientific), hexamethylenetetramine (HMT, Alfa Aesar), KOH (semiconductor grade, Sigma-Aldrich), highly oriented pyrolytic graphite (HOPG, 12 mm × 12 mm × 2 mm, ZYB grade, Bruker), Epoxy (Loctite Hysol 1C).

Synthesis of dodecyl sulfate intercalated $Ni(OH)_2$ (DS-$Ni(OH)_2$). $Ni(OH)_2$ intercalated with dodecyl sulfate (DS) was synthesized through a hydrothermal method as reported previously.[1] Briefly, DS-$Ni(OH)_2$ was synthesized by precipitation of an aqueous solution containing Ni^{2+} and sodium dodecyl sulfate (SDS). 0.5 M $Ni(NO_3)_2 \cdot 6H_2O$, 0.25 M SDS, and 1 M HMT stock solutions in water were prepared. Then, 0.9 ml Ni^{2+}, 9 ml SDS, and 2.7 ml HMT were added into 45 ml Parr-bomb container filled with 10 ml ultrapure water. The sealed Parr-bomb container was placed at 120 °C in an oven for 24 h. The precipitates obtained after the hydrothermal process were centrifuged, decanted, and washed with water and ethanol four times. The DS-$Ni(OH)_2$ was obtained after drying at room temperature.

Synthesis of Single-layered $Ni(OH)_2$ (SL-$Ni(OH)_2$). 5 mg of DS-$Ni(OH)_2$ was dispersed in 10 ml formamide and placed in an oven at 40 °C for 5 days to drive exfoliation. Subsequently, the suspension was centrifuged (2,000 rpm for 30 min), and the supernatant was transferred into a clean tube and centrifuged again (10,000 rpm for 30 min). The sediments were then rinsed with ultrapure water twice and collected

via centrifugation (13,000 rpm for 30 min) each time. Finally, the product was suspended in 5 ml ethanol and was used as the SL-$Ni(OH)_2$ dispersion.

In-situ electrochemical atomic force microscope (in-situ AFM)

Cell construction. The baseplate of the cell is made from Teflon. The constitution of the cell is presented in Figure S5. The cell is designed to allow the use of a standard Ag/AgCl reference electrode.

Fabrication of working electrodes. HOPG was chosen as the substrate because of its electronic conductivity and atomically flat surface. 50 µl of the SL-$Ni(OH)_2$ dispersion were dropped on HOPG (after cleaving with Scotch tape to reveal a new surface) and spun for 30 s at 3,000 rpm. Then the HOPG with SL-$Ni(OH)_2$ was placed on a hot plate and heated at 180 °C for 1 h. The HOPG was then mounted in the sample holder of the homemade cell with Cu tape and an electrical contact was made to the HOPG with Cu wire. Epoxy was used to cover the contact (Cu wire and Cu tape) and keep it isolated from solution. The cell was ready for in-situ AFM test after cell assembly with an o-ring, cover glass (Bruker, EC-V2-COVER GLASS), o-ring with Pt wire (for the counter electrode), plastic ring, and the Ag/AgCl reference electrode.

In-situ electrochemical AFM measurements (EC-AFM). Electrochemical measurements were conducted in a customized cell (described above) containing 3.5 ml 0.1 M KOH electrolyte (semiconductor grade, diluted with ultrapure water, and filtered through a 200-nm filter membrane, Whatman). While this electrolyte is known to contain trace Fe[2,3], the low levels are unlikely to affect the morphology dynamics. Fe-free electrolytes can be obtained by procedures described previously, but these electrolytes contain trace Ni that can itself deposit on the electrode surface, making them unsuitable for the study conducted here. A BioLogic SP-300 potentiostat with low current density probe was used for measurements. A saturated Ag/AgCl was used as the reference electrode and Pt wire as the counter electrode. The AFM images were collected on a Bruker Dimension Icon using ScanAsyst-fluid probe (Bruker) in EC-ScanAsyst mode during the electrochemistry measurement.

Materials characterization. Scanning electron microscope (SEM) images and energy dispersive X-ray spectroscopy (EDX) data were collected using a FEI Helios 600/600i FIB-SEM operating at 4 KeV and atomic force microscope (AFM) images were taken on a Bruker Dimension Icon using a Tespa v2 probe in FastScan mode for ex situ measurements. A ScanAsyst-fluid (Bruker) probe was used for in-situ AFM measurements using EC-ScanAsyst mode. Grazing-incidence GIXRD patterns were collected on a Rigaku SmartLab diffractometer. Relative compositions of nickel and sulfur were quantified using a Rigaku Primus II X-ray fluorescence (XRF) spectrometer with a rhodium source. Fluorescence counts were integrated with background subtraction based on counts recorded using a bare silicon substrate.

Data collection and analysis. The effective surface area and the mean height of the nanoplatelets was collected using the "Roughness" function in the NanoScope Analysis. The specific region chosen was the

smallest square that encompassed the entire nanosheet. The volume of the nanoplatelet was collected using the “Bearing Analysis” function in the NanoScope Analysis within the specific chosen region in the AFM images. The redox capacity was calculated by integration of the Ni oxidation wave and normalized to the electrode area.

Supporting Results

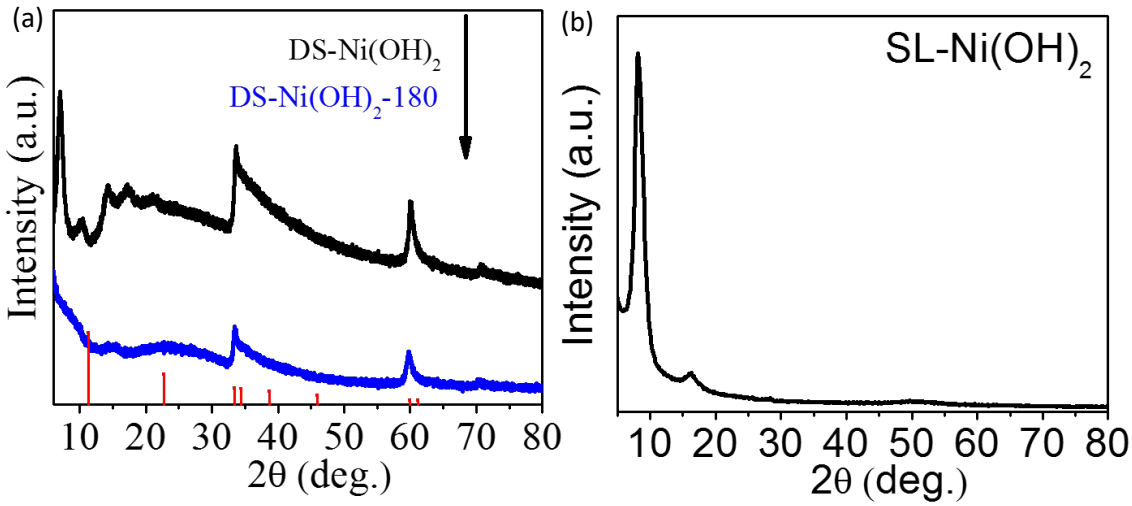

Figure S1. (a) X-ray diffraction patterns of the DS-$Ni(OH)_2$ without annealing process, and DS-$Ni(OH)_2$-180 annealed in 180 °C for 1 h (blue). (b) Grazing-incidence GIXRD patterns of the SL-$Ni(OH)_2$ annealed in 180 °C for 1 h. The reference stick pattern is for α–$Ni(OH)_2$.

Hexamethylenetetramine was used drive the precipitation of Ni^{2+} and sodium dodecyl sulfate to prepare the DS-$Ni(OH)_2$ under the hydrothermal conditions. Diffraction peaks (Figure S1a) at ~ 14°, 33° and 60° correspond to the (003), (101), and (110) planes of the α–$Ni(OH)_2$ (JCPDS 380715). The peak at 8° is likely associated with the extended basal spacing (2.7 nm) because of the intercalation of dodecyl sulfate ions (DS).[1] After annealing the powder at 180 °C for 1 h the peak at 8° decreases in intensity and broadens. Figure S1b shows a diffraction pattern from powders of the exfoliated samples also annealed at 180 °C for 1 h. Interestingly, a large low-angle peak is present suggesting the single layers restack when precipitated as powders.[4]

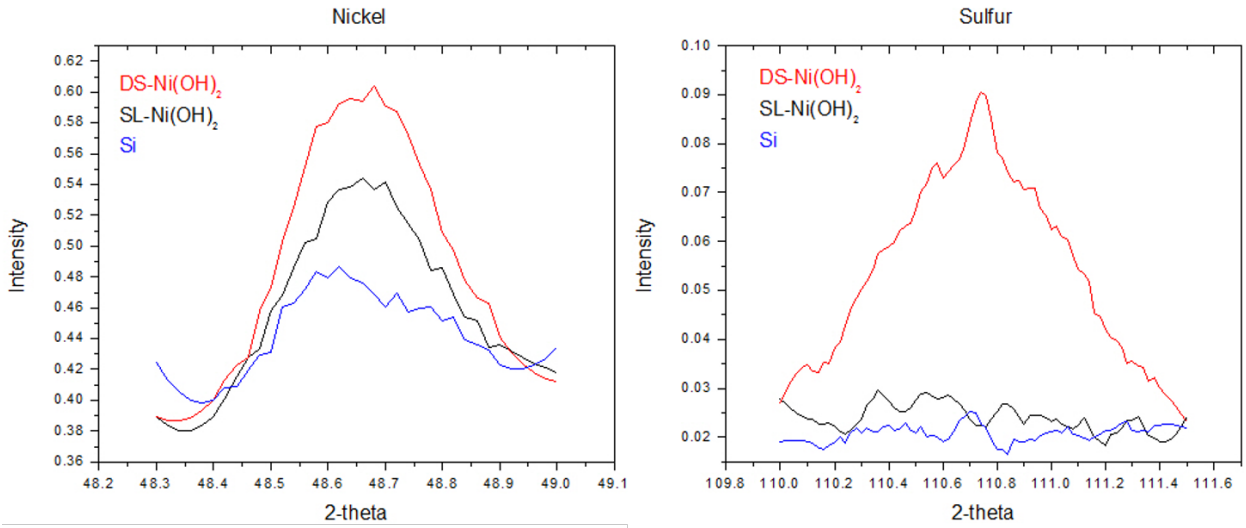

Figure S2. XRF spectra of layered nickel hydroxide intercalated with dodecyl sulfate ions (DS-$Ni(OH)_2$), the exfoliated SL-$Ni(OH)_2$, and a bare Si wafer (which was used a substrate for the measurement and hence serves as a good baseline). The S signal for the exfoliated samples are near the noise level for the measurement, as indicated by the similarity to the Si baseline signal. This indicates removal of the surfactant during the exfoliation process.

Table S1 Ratio of Ni/S baseline-corrected integrated counts from XRF spectra

Material	Ni:S counts
DS-$Ni(OH)_2$	0.6 : 1
SL-$Ni(OH)_2$	6.8 : 1

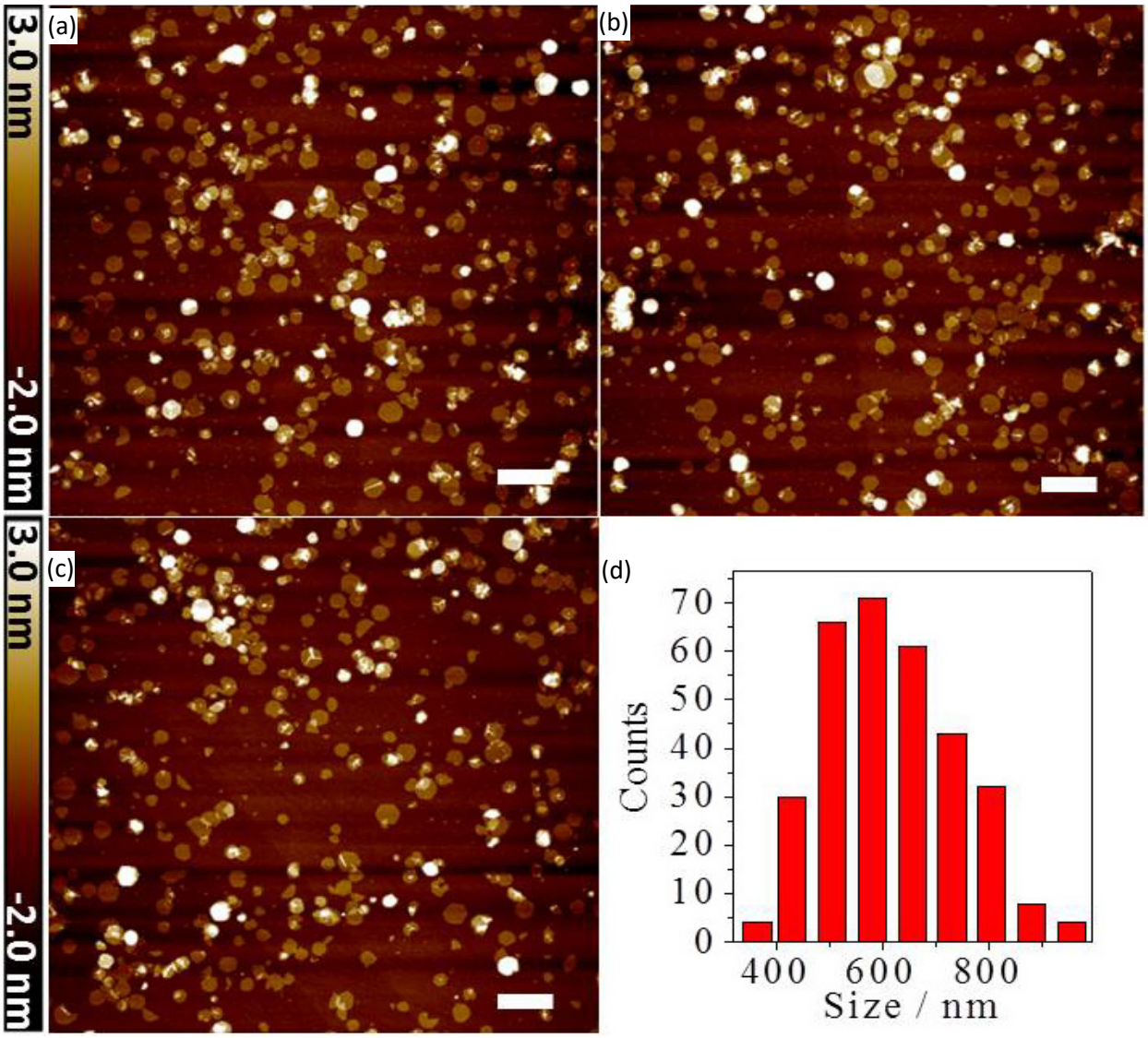

Figure S3. (a), (b), (c) AFM images of SL-Ni(OH)$_2$ on a Si wafer (the scale bar is 2 μm). (d) Size statistics of the SL-Ni(OH)$_2$. The mean diameter is ~ 600 nm.

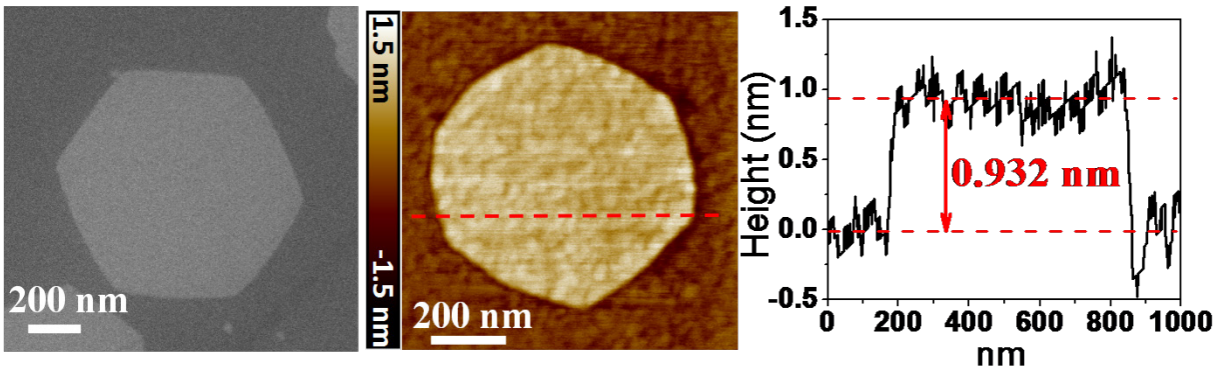

Figure S4. (a) SEM image of the SL-$Ni(OH)_2$ on HOPG. (b) AFM image of the SL-$Ni(OH)_2$ on a Si wafer collected with tapping mode. (c) height of the SL-$Ni(OH)_2$ with the red line section in Figure S3b. The SEM image along with the AFM image indicate the formation of single-layered $Ni(OH)_2$ with hexagonal shape.

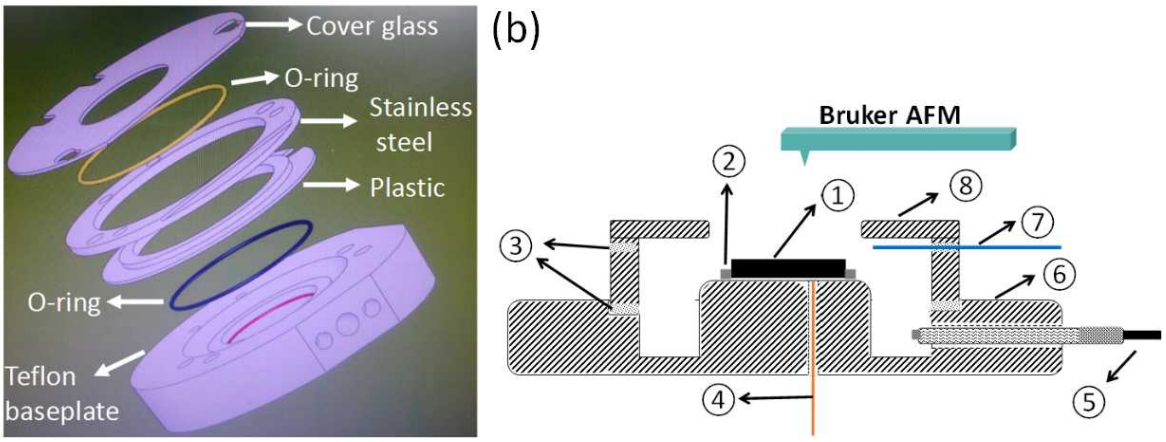

Figure S5. (a) Constitution of the EC-AFM cell. (b) Schematic of the cell (mounted with HOPG) for in-situ AFM (① HOPG ② epoxy ③ O-ring ④ Copper wire ⑤ Ag/AgCl reference electrode ⑥ Teflon ⑦ Pt wire (counter electrode) ⑧ Cover glass (Bruker, EC-V2-COVER GLASS))

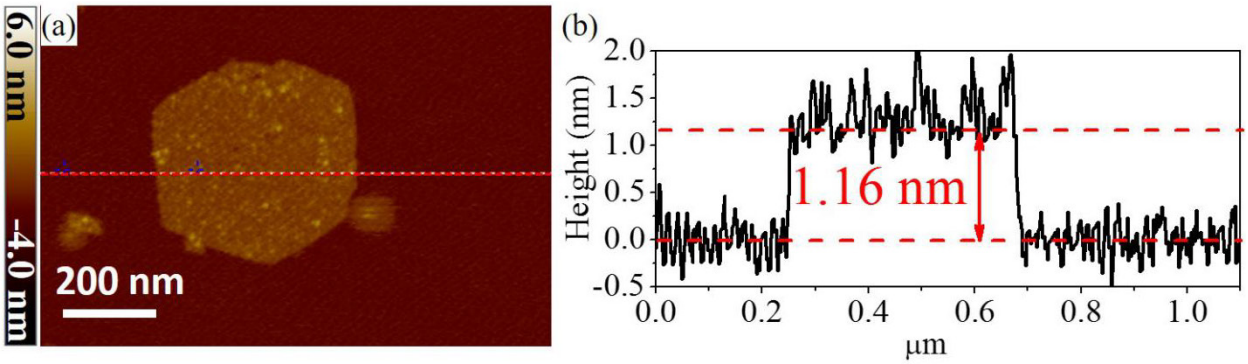

Figure S6. (a) AFM image of the SL-$Ni(OH)_2$ in 0.1 M KOH at the OCV on HOPG. (b) Height of the SL-$Ni(OH)_2$ across the red line in Figure S5a. The height of the SL-$Ni(OH)_2$ in the 0.1 M KOH is 1.16 nm which is slight higher than that in the air, presumably due to hydration "underneath" the nanosheet.

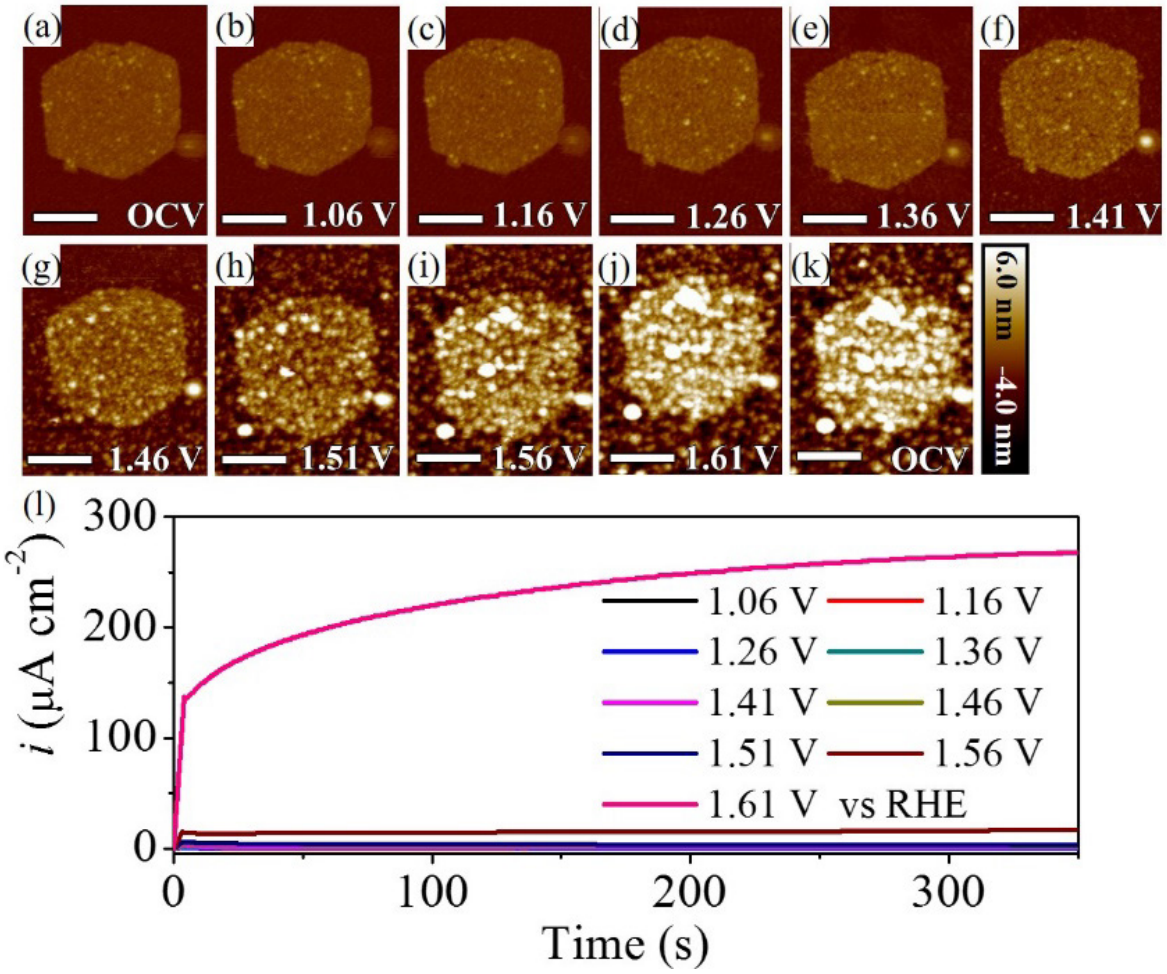

Figure S7. AFM images of SL-$Ni(OH)_2$ with different potentials applied within EC-scanasyst mode; the scale bars are 200 nm. Figure S6 (a - k) have the same scale bar of the height and the scale bar. (l) Current-time (*i-t*) chronoamperometric responses at different constant applied potential. These results show that the dramatic restructuring is associated with the onset of Ni oxidation and driven more rapidly as the OER current turns on at 1.56 V vs RHE.

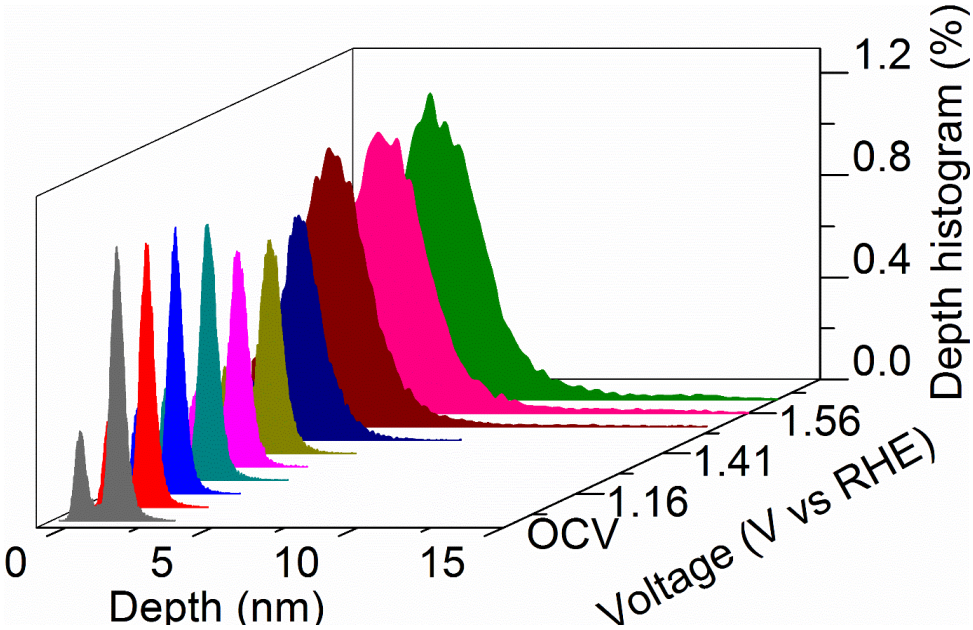

Figure S8. Depth histogram of the SL-$Ni(OH)_2$ at different potentials. This figure indicates the size distribution of the nanosheets shifts to higher values as the potential increases.

Formation of particles. The HOPG substrate (on which the nanosheet sits) was clean in the initial electrode and there were no changes until the potential was increased to 1.41 V vs RHE (Figure S7f). The AFM images show that small nanoparticles suddenly emerged on the previously bare substrate at 1.41 vs RHE. The nanosheets themselves transform into nanoparticles completely at the 1.56 V vs RHE (Figure S7g) and larger features appear at higher potential. Additionally, the nanoparticles adsorbed on the surrounding substrate at 1.41 V vs RHE increase in size and number at higher potentials. The current at 1.56 V vs RHE is dramatically increased due to the enhancement in conductivity when $Ni(OH)_2$ transformed into NiOOH and the catalyst starts to drive the OER reaction (Figure S7l).

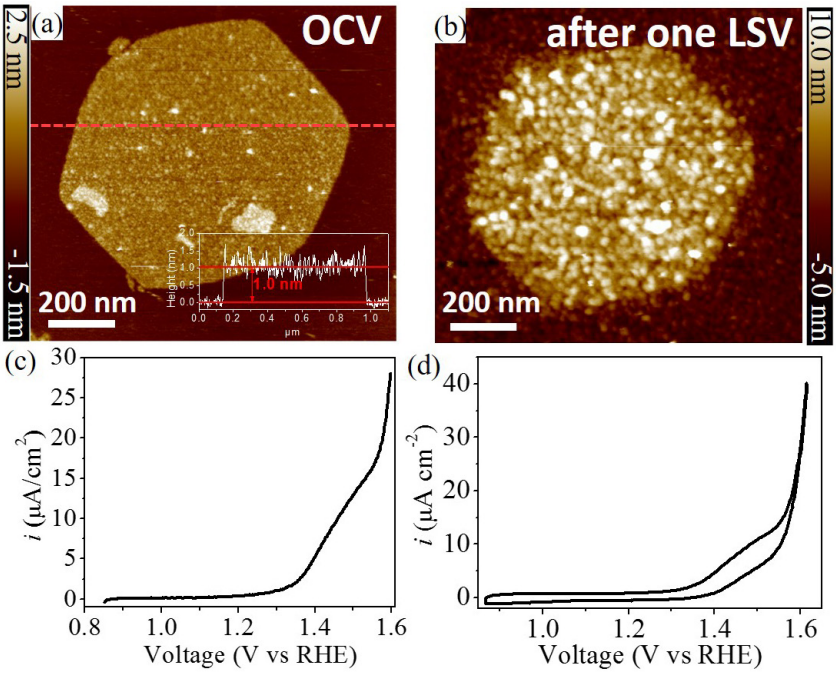

Figure S9. (a) AFM image of a SL-$Ni(OH)_2$ nanosheet on the HOPG in 0.1 M KOH at OCV. (b) AFM image of a SL-$Ni(OH)_2$ after one cycle of linear sweep voltammetry as in Figure S9c from 0.86 to 1.61 V vs RHE. (c) Linear scan voltammetry curve from 0.86 V to 1.61 V vs RHE with the scan rate of 1.5 mVs^{-1}. (d) CV curve of the electrode based on SL-$Ni(OH)_2$ after the first LSV. The nanosheet converts into nanoparticles after the initial LSV but little reversible redox chemistry is observed, suggesting not all of the Ni species are yet in good electrical contact with the electrode.

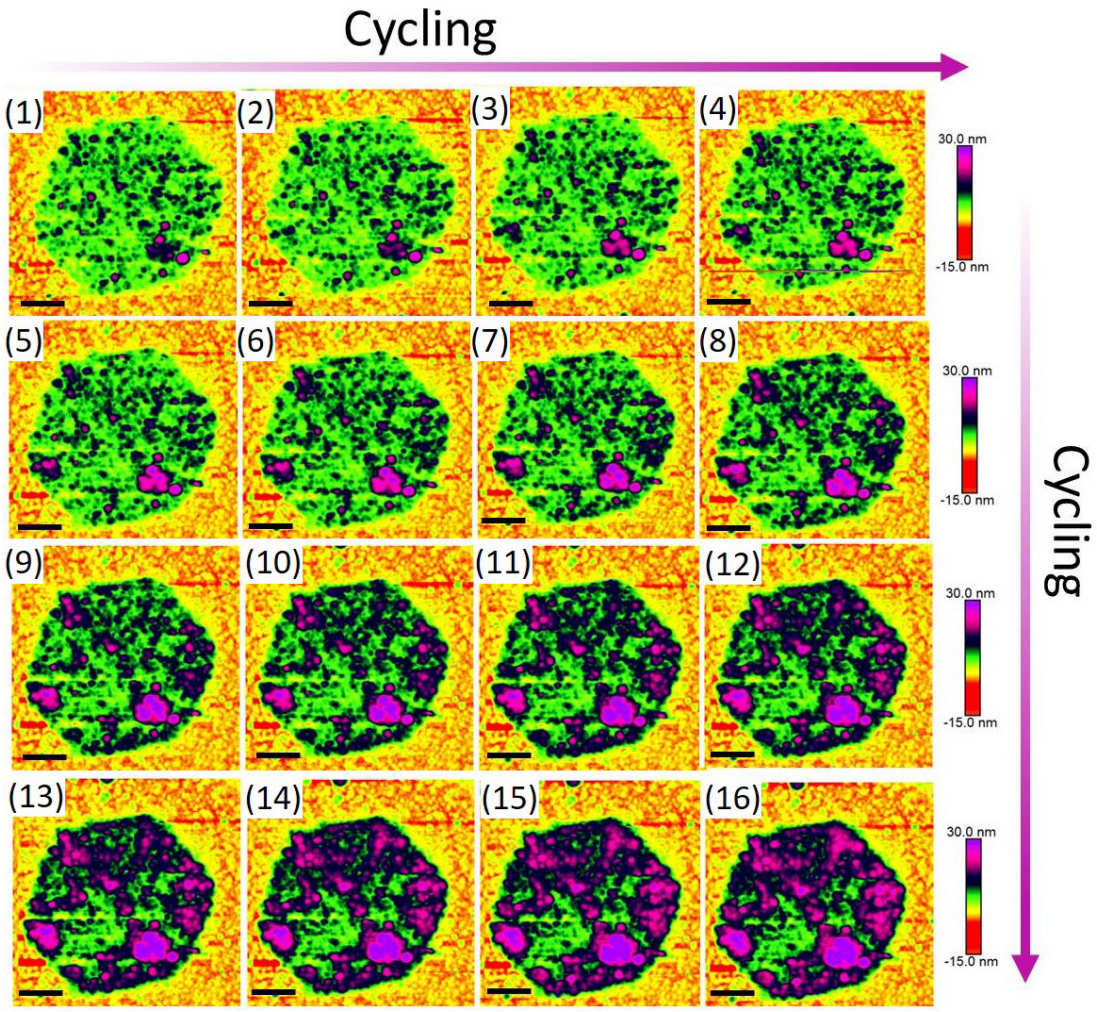

Figure S10. AFM images during the cyclic voltammetry process (scale bars = 200 nm). Some regions in the nanosheet preferentially grow higher during the electrochemical conditioning.

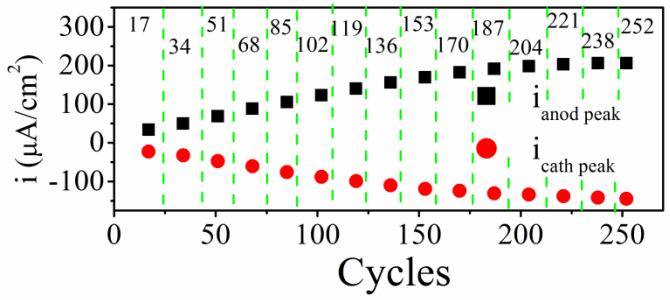

Figure S11. The peak current during the multiple CV processes. The redox peak grows gradually and then reaches a plateau associated with full electrochemical activation of the SL-Ni(OH)$_2$.

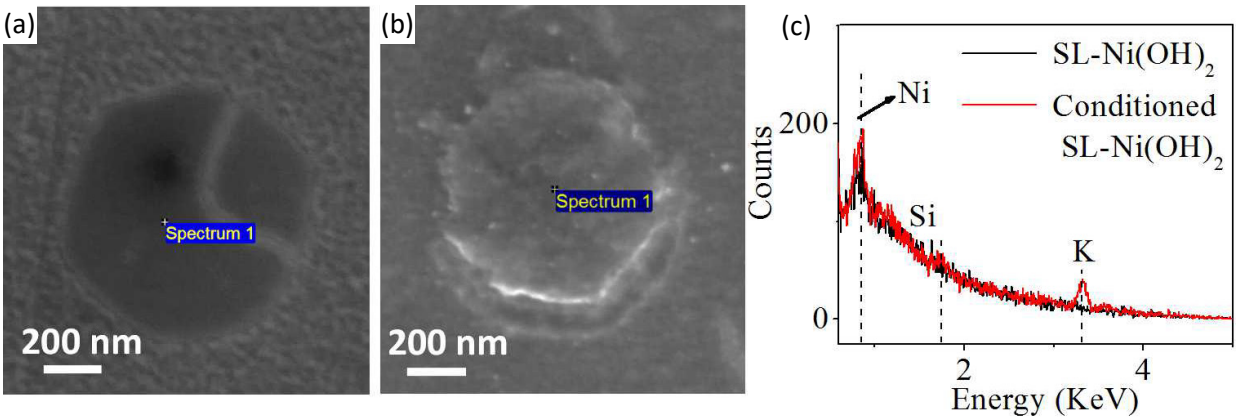

Figure S12. SEM images of (a) SL-Ni(OH)$_2$ and (b) conditioned SL-Ni(OH)$_2$. (c) EDX spectra of the nanoplatelets as indicated in panels a and b. The SEM images show the nanosheets maintain a hexagonal shape after several CV cycles but acquire a rough surface. The EDX data show that the absolute amount of Ni does not change substantially after the cycling process.

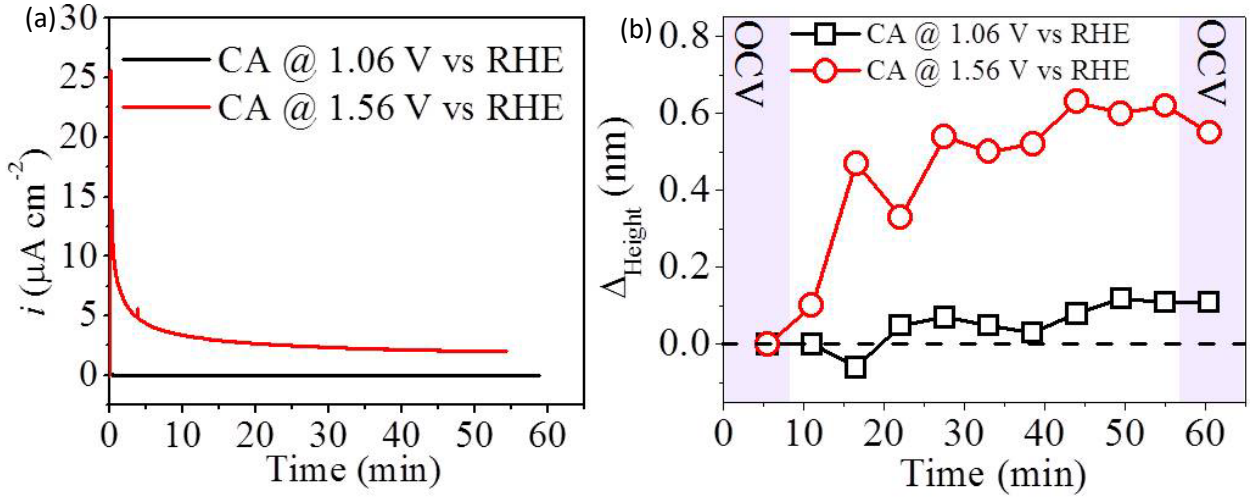

Figure S13. (a) Current-time (*i-t*) chronoamperometric responses at constant potential of 1.06 V and 1.56 V vs RHE, respectively. (b) Corresponding mean height change of the SL-Ni(OH)2 nanoplatelet versus time.

As shown in Figure S13a, there is a negligible current at 1.06 V vs RHE. The current increases dramatically during the Ni(OH)$_2$/NiOOH transition at 1.56 V vs RHE and reaches a steady state associated with the OER. The mean height of the nanoplatelet only increases slightly with time when a voltage of 1.06 V vs RHE was applied (Figure S13b). However, once a voltage of 1.56 V vs RHE is applied, the mean height increases substantially in the first 15-30 min and then remains mostly unchanged. This initial response is ascribed to the breaking of the nanoplatelet and subsequent reorganization as described in the manuscript.

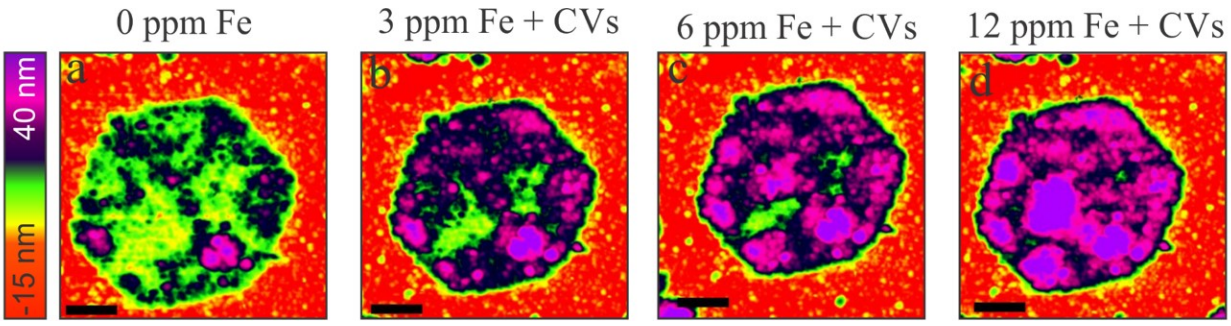

Figure S14. (a-d) AFM images of the nanoplatelet in 0.1 M KOH in presence of 0, 3, 6, and 12 ppm Fe and after three CVs. The addition of the larger Fe concentrations results in much higher features in the $Ni(OH)_2$ which suggests that separate FeOOH deposits on top of the NiOOH under such conditions.

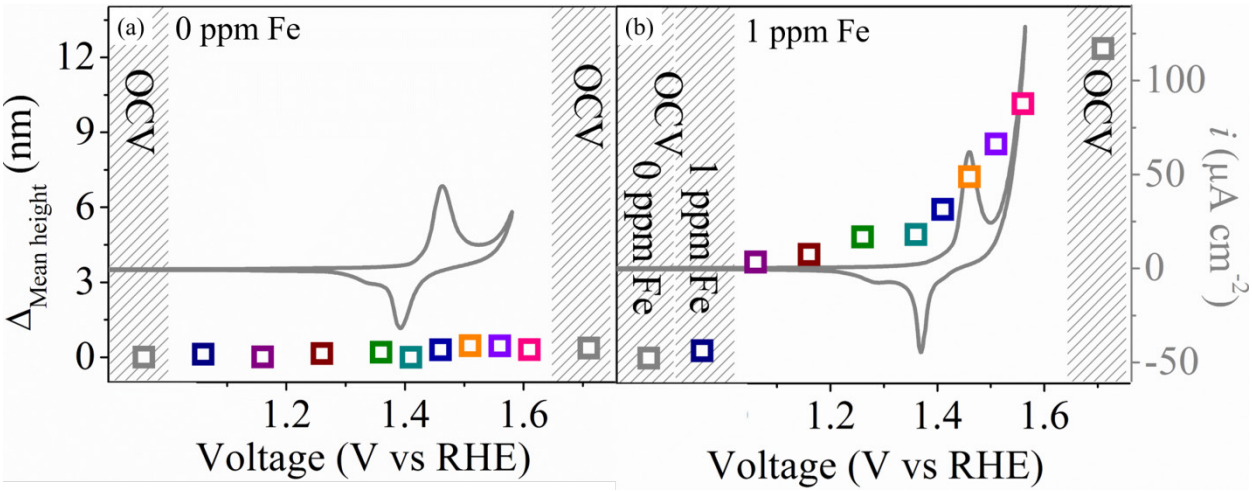

Figure S15. Mean height of the nanosheet at varying potentials (a) in absence of Fe after hundreds of CV cycles recorded until the redox peak did not further change; and (b) subsequently adding 1 ppm Fe into the 0.1 M KOH. CV curves (scan rate of 10 mV s^{-1}) of the HOPG/SL-$Ni(OH)_2$ system without or with Fe is presented as the background (grey). The data shows the dramatic increase of mean height occurred in the presence of Fe once the sufficient anodic potential was applied.

References

(1) Ida, S.; Shiga, D.; Koinuma, M.; Matsumoto, Y., *J Am Chem Soc* **2008,** *130*, 14038-14039.
(2) Corrigan, D. A., *J. Electrochem. Soc.* **1987,** *134*, 377-384.
(3) Trotochaud, L.; Young, S. L.; Ranney, J. K.; Boettcher, S. W., *J. Am. Chem. Soc.* **2014,** *136*, 6744-6753.
(4) Hall, D. S.; Lockwood, D. J.; Bock, C.; MacDougall, B. R., *Proc. R. Soc. A* **2015,** *471*.